PHYSICAL REVIEW A VOLUME 18, NUMBER 1 JULY 1978

Millimeter spectroscopy in sodium Rydberg states: Quantum-defect, fine-structure, and polarizability measurements

C. Fabre and S. Haroche
Laboratoire de Spectroscopie Hertzienne de l'ENS, 24, rue Lhomond, 75231 Paris Cedex 05, France

P. Goy
Groupe de Physique des Solides de l'ENS, 24, rue Lhomond, 75231 Paris Cedex 05, France
(Received 14 June 1977)

Millimeter resonances corresponding to single- and double-photon transitions have been observed between Rydberg levels of sodium with principal quantum number n ranging from 23 to 41. The levels are prepared by laser excitation; transitions are induced by microwaves produced by a backwave oscillator working around 300 GHz; detection is performed through the selective field-ionization technique. Experimental values for quantum defects, fine-structure intervals, and polarizabilities are reported.

I. INTRODUCTION

Microwave transitions in atomic Rydberg levels have been up to now restricted to measurements of energy intervals in the centimeter frequency range between states belonging to the same electronic shell[1,2] ($\Delta n = 0$ transitions, $n \lesssim 20$). These experiments have allowed very precise determinations of quantum defects[1] and fine-structure intervals.[1,2] The advantages of extending experiments to $\Delta n \neq 0$ transitions has been recently pointed out by Kleppner in discussing a possible new determination of the Rydberg constant.[3]

To study microwave-induced $\Delta n \neq 0$ transitions, one can either extend the above mentioned centimeter resonances to levels much closer to the ionization limit ($n \sim 60$) or study millimeter resonances on less excited Rydberg levels ($\Delta n = 1, 2$ transitions for $n \sim 30$–40). This latter choice seems more attractive, since moderately excited Rydberg states ($n \sim 30$) are less sensitive to electric field perturbations and hence better candidates for accurate spectroscopic investigations. Furthermore, the interaction time between the atoms and the microwave being limited by the size of the setup to values practically independent of the frequency, it is better, in view of the ultimate resolution of the experiment, to study the highest possible microwave frequency transitions.

We have chosen to investigate such transitions near 300 GHz, where a tunable (±6% in frequency) powerful microwave source is available. Although the ultimate precision of this technique should be very high, direct frequency measurements in this range are much more difficult than in the centimeter band. They involve the use of a frequency multiplying chain allowing one to compare via heterodyne mixing the millimeter frequency of interest with a harmonic of a stabilized centimeter klystron. Such precise frequency measurements are now being developed in our laboratory. In the mean time, however, it has been very easy to get a moderate resolution of about 10^{-4} by direct measurement of the millimeter wavelengths. Within this resolution, a lot of interesting spectroscopic investigations can be performed.

We report in this paper preliminary determinations of millimeter transitions between Na Rydberg states with principal quantum number n in the range 23–41 and angular momentum l in the range 0–3 (s, p, d, f states). Single- and double-quantum transitions with $\Delta n = 0, 1, 2$, $\Delta l = 0, \pm 1$ have been observed. These measurements yield values of quantum defects, fine-structure intervals (for np levels), and scalar and tensor polarizabilities.

II. EXPERIMENTAL TECHNIQUE

The principle of the microwave double-resonance experiment has been briefly described in a previous Letter.[4] The general scheme of the setup is recalled in Fig. 1(a). The Na atoms, propagating in an atomic beam, are prepared by stepwise pulsed laser excitation in an nS or nD state. They are irradiated by the CW microwave field produced by a C010 Thomson – CSF backwave oscillator (BWO). This irradiation produces single-photon nS-$n'P$, nD-$n'P$, nD-$n'D$, and two-photon nS-$n'S$ transitions. Monitoring of these transitions is achieved through detection of the electrons produced by ionization of the Rydberg atoms with a pulsed electric field applied at a given delay after the laser excitation. Let us now review in more detail the various aspects of the experiment.

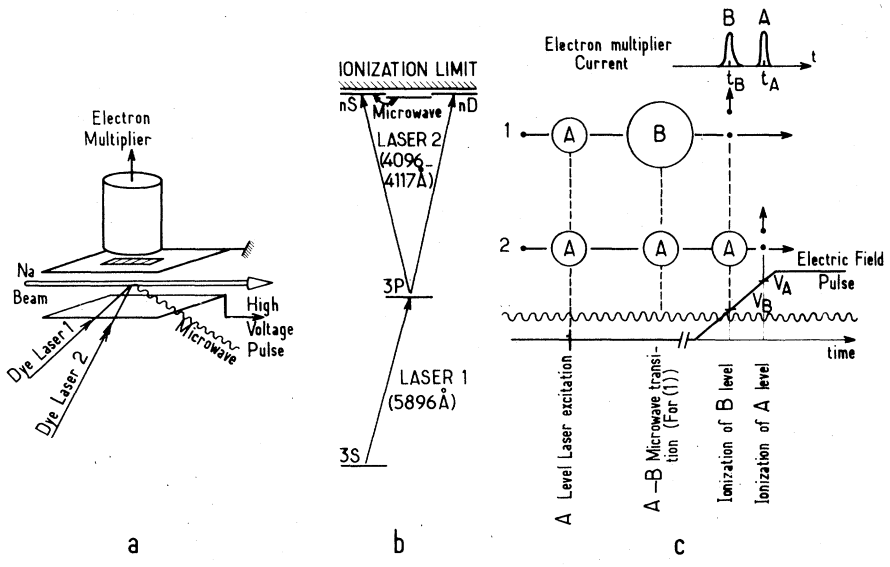

FIG. 1. (a) Scheme of the experimental setup. (b) Energy diagram of the Na atom showing the levels populated by the laser stepwise excitation and the microwave transitions. (c) Sketch representing the sequence of events experienced by Na atoms.

A. The atomic beam

The atomic beam is produced by an oven heated to about 350 °C. The collimation ratio r ($\simeq 30$) does not need to be good, since the spectroscopic resolution is not limited by the Doppler effect. The atomic density in the excitation region is on the order of 10^{11} atoms/cm^3. The background gas pressure is on the order of 10^{-6} Torr and is low enough to ensure a mean free path of at least a few mm for the Rydberg levels of interest. Such a mean free path is long enough for our experiment, since the interaction with the microwave field lasts only a few microseconds (see below).

B. Preparation of the "initial" Rydberg state

The initial Rydberg state of the millimeter transition is prepared by two N_2 laser-pumped-dye laser pulses via the well-known stepwise process [see Fig. 1(b)]. The first pulse tuned at $\lambda_1 = 5896$ Å pumps the atoms to the $3P_{1/2}$ level. A second synchronous pulse then excites the $3P_{1/2}$-nS or $3P_{1/2}$-nD transition (its wavelength λ_2 ranging from 4117 to 4096 Å for n varying from 23 to 39). Matching of the laser frequencies to resonance is achieved with the help of a high-resolution grating spectrometer ("gross" tuning) and by monitoring the ionization current obtained by field ionization of the Rydberg levels ("fine" tuning; see Sec. II C). The laser pulses have a duration of about 2 nsec and follow each other at a 1-nsec delay, so that the excitation may be considered as instantaneous with respect to all time constants of the excited levels (lifetime of Rydberg states ~ several tens of microseconds).

The spectral width of the lasers is about 0.1 Å (10–15 GHz) and is narrow enough to allow an unambiguous and selective excitation of all the nS and nD levels in the range $n = 23$–41. [$3P_{1/2}$-nS and $3P_{1/2}$-$(n+1)S$ transitions are about 1 Å apart for $n \sim 40$.] The λ_1 laser peak power is about 1 kW/mm^2 and the λ_2 laser one is about 50 kW/mm$_2$. (The power of the second laser is boosted by placing in front of it an amplifying cell pumped by a part of the beam of the N_2 laser.) These powers are large enough to ensure complete saturation of the $3S_{1/2}$-$3P_{1/2}$ line and also saturation at least for the lower $3P_{1/2}$-nS and $3P_{1/2}$-nD transitions ($n \sim 25$). The oscillator strengths decreasing as n^{-3}, the highest $3P_{1/2}$-nS or $3P_{1/2}$-nD transitions are certainly not saturated, but a non-negligible ratio (~ 0.01 at least) of atoms should be nevertheless transfered to nS or nD levels ($n \sim 40$). From the measurement of the field ionizing current (see below), one can estimate that 10^4–10^5 atoms at least are prepared in a well-defined Rydberg level by each laser excitation process.

C. Transition between the "initial" and the "final" Rydberg states

Immediately after excitation, the Rydberg atoms start to interact with the microwave field. This field is coupled to the atomic beam apparatus through a Mylar window placed at the end of a millimeter waveguide which brings the microwave directly from the BWO. The resonant interaction between the atoms and the microwave lasts a variable time interval of about 2 to 5 μsec; after that delay, detection takes place and interrupts the coherent interaction between the atoms and the

field (see Sec. II D). During the interaction time, the atoms' propagation along the beam is very small (1 to 2 mm) compared to the size of the apparatus, so that the laser excitation, the microwave irradiation, and the detection practically occur at the same spatial point in the beam.

The microwave oscillator is tunable from 277 to 313 GHz. In that relatively wide range of frequencies, one finds a large number of allowed single- and double-quantum transitions between Rydberg levels in the $n = 23-41$ range (see Sec. III).

The frequency of the BWO is tuned by sweeping its high-power supply voltage V (V varies between 3300 and 6000 V). The slope of frequency versus voltage depends on the working point of the oscillator. A typical slope is about 10 MHz/V. Day-to-day reproducibility of the frequency for a fixed voltage corresponds to a few tens of MHz. Short-term stability of the BWO at a given voltage is of the order of 1MHz, but could certainly be improved by frequency-locking it to a high-Q external cavity (improvement in progress). Absolute frequency calibration of the microwave relies, for the time being, on wavelength interferometric measurements: Part of the microwave signal is sent through a high-Q millimeter tunable semi-cofocal Fabry-Perot etalon whose transmission is monitored by a He-cooled bolometric detector.

Displacement of the fringes while sweeping the cavity (or the voltage of the carcinotron) allows determination of the wavelengths with a precision of about 10^{-4} (30 MHz absolute uncertainty). Frequencies are determined with the same precision, provided one knows the speed of light for millimeter radiation in air, c_{air}. In order to obtain c_{air} around 300 GHz (which is not available in usual handbooks) we have made a direct measurement of the refraction index of air at 303 GHz by looking at the shift of the fringes when the Fabry-Perot cavity is pumped out. We have obtained

$$n - 1 = (2.72 \pm 0.06) \times 10^{-4}, \quad (1)$$

and hence

$$c_{air} = 2.997\,11 \times 10^{8} \text{ m/sec} \quad (2)$$

in our room conditions (around 25 °C and 50% humidity).

The BWO power lies between 10 and 50 mW. This power is spread at the atomic beam location over a surface of a few cm^2, so that the maximum microwave flux at the interaction point may be evaluated to about 10^{-2} W/cm^2 (this corresponds to a maximum oscillating electric field of about 2 V/cm). Attenuators placed on the waveguide can reduce this power to 10^{-9} or 10^{-10} W/cm^2. The power level needed to saturate the single-photon resonances ranges from 10^{-10} to 10^{-6} W/cm^2 depending on the oscillator strength of the transition. For two-photon transitions, a power of the order of 10^{-3} W/cm^2 is required. These low power levels are due, of course, to the very large values of the electric dipole matrix elements between Rydberg levels, which scale as n^2.

D. Detection of the "final" Rydberg state

Detection of the resonance is made by the selective field ionization technique described in our previous Letter[4] and already developed under slightly different forms in various recent experiments.[5-8]

We have represented in Fig. 1(c), as a function of time, the sequence of events experienced by the atoms. At time $t = 0$, the laser excitation occurs. During the time interval ΔT the atoms interact coherently with the microwave. At time ΔT, an electric-field ramp (maximum field value $\simeq 1.2$ kV/cm) is applied to the atoms, in order to ionize them and produce an electric signal at the output of an electron multiplier. The threshold electric field for ionization varies according to a n^{-4} law[5] and hence depends on the Rydberg level of interest. The electric field thus reaches at two slightly different times the values corresponding to ionization of the two states connected by the transition of interest. We have symbolized in Fig. 1(c) the "history" of two atoms 1 and 2, one undergoing the microwave transition and the other not. Before laser excitation both atoms are in the ground state and are represented by very small points. At $t = 0$, they are both excited in the initial Rydberg state A, and thus become two large identical "balls." At a given time, atom 1 undergoes the microwave transition $A \rightarrow B$, which we suppose here to be an upward transition (absorption of microwave quantum) and thus its size slightly increases. Atom 2 is supposed to remain in its initial Rydberg state A. These two atoms will then behave differently in the saw-tooth-shaped detection field: Ionization threshold will be reached first at a time t_B for the bigger atom 1, and this atom will contribute to an electron signal peak around t_B. The threshold for the smaller atom 2 will be reached at a larger field, corresponding to a latter time t_A, and this atom 2 will contribute to a signal peak around t_A. The initial and final states of the transition will thus give rise to two time-resolved ionization signals.

Figure 2 shows a typical example of such signals: Trace (a) corresponds to the ionization versus time signal from level 23S, when there is no microwave irradiation. Trace (b) corresponds to the signal observed in the same conditions when

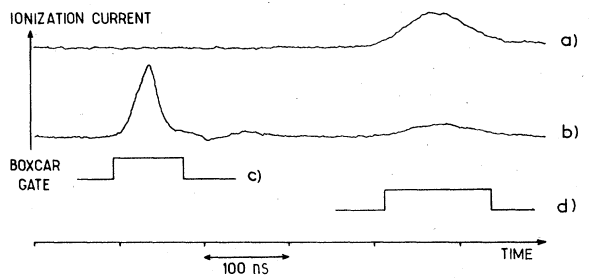

FIG. 2. (a) and (b) ionization signals as a function of time without [trace (a)] and with [trace (b)] microwave irradiation (study of the 23S-23P microwave transition). (c) and (d) positions of the boxcar gate which yield a resonant signal.

a microwave field resonant for the 23S-23P transition is switched on. One clearly observes a new resonant feature corresponding to resonant population of the more excited 23P level, and a depletion of the 23S signal. Either peak can be isolated from the other and averaged over a few tens of runs with the help of a PAR 162 boxcar integrator whose gate is placed around t_B or t_A [traces (c) and (d) of Fig. 2 show the boxcar gate positions]; the resonance can thus be detected either by an increase of the signal corresponding to the final state B of the transition [boxcar gate in (c) in Fig. 2] or by a decrease of the signal corresponding to its initial state A [boxcar gate in (d)].

Let us also notice that this detection technique should apply not only for microwave transitions but also for studying any physical process transferring the atoms from a Rydberg level to another one: We have in that way obtained evidence for collisional transfers occurring when the vacuum in the atomic beam is not very good (above 10^{-5} Torr): one then observes, beside the peak corresponding to the level excited by the laser, one or several side peaks corresponding to easily identified nearby Rydberg states. These states are obviously populated by collisions with the background gas. These collisions could in that way be studied in detail. The selective-field-ionization detection technique acts thus as a kind of "Rydberg atom spectrometer" which could be used in a lot of interesting studies on these atoms.

E. Example of observed resonances: The "23S-23P-24S triangle"

We discuss in this subsection, as a typical example of the possibilities of the method, the results obtained on a given set of Rydberg levels, the 23S-23P-24S triangle displayed in Fig. 3. (The fine structure of the P level is magnified by a factor of 100 in the insert of this Figure.) In this configuration, one can observe two single-photon transitions (23S → 23P and 24S → 23P) and a double-photon transition (23S → 24S) occurring at half the frequency sum of the single-photon transitions. These resonances are displayed on the recording of Fig. 4.

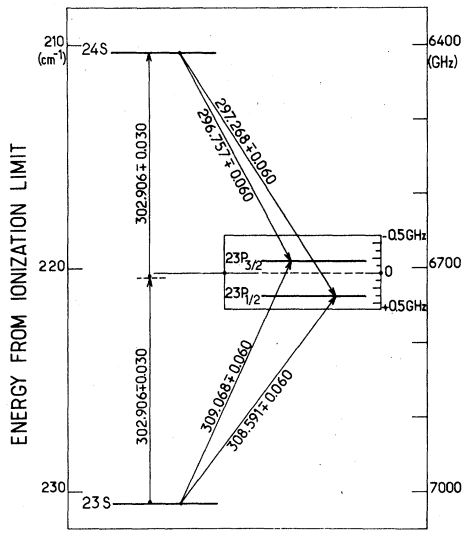

FIG. 3. "23S-23P-24S triangle" (the scale in the insert is magnified by a factor of 100).

1. Single-photon S-P transitions

By exciting the 23S or 24S level and monitoring the 23P level population, one obtains the resonances displayed on parts (a) and (c) of Fig. 4. Both 23S-23P and 24S-23P transitions exhibit the splitting due to the 23P-level fine structure. It is interesting (for example for quantum-defect measurements, see Sec. IIB) to determine the positions of the resonances when the effect of the fine-structure coupling is "removed." It is easy to show that the

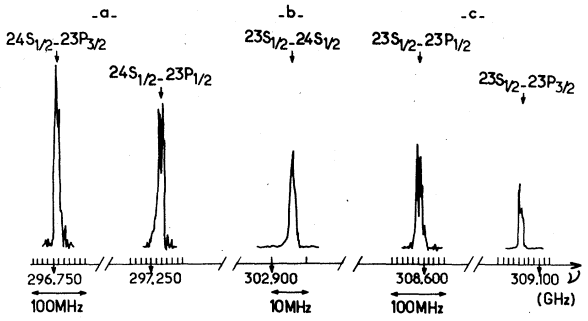

FIG. 4. Ionization current as a function of the BWO frequency showing different resonances: (a) and (c) fine-structure lines on the transitions 24S-23P (a) and 23S-23P (c); (b) two-photon 23S-24S line recorded with an expanded frequency scale and a microwave power 10^7 times greater than in (a) and (c).

positions of the resonances "without fine structure" would lie at one-third of the fine-structure interval, on the side of the $P_{3/2}$ line. Because of the very large electric dipole matrix elements linking the S and P levels when Δn is 0 or 1, the transitions are saturated by very weak microwave intensities. We have detected the $23S$-$23P$ transition with a microwave attenuation of 85 dB, corresponding to a microwave power smaller than 10^{-10} W/cm^2. The ultimate width of the resonance is of the order of 6 MHz and is limited by the Stark broadening due to the stray electric-field inhomogeneities (~200 mV/cm). Furthermore, each resonance line is split into two peaks separated by 3 to 4 MHz. This extra splitting is due to the Zeeman effect in the magnetic field leaking from the BWO magnet, placed 1 m away from the interaction region.

2. *Two-photon S-S transition*

The large values of the dipole matrix elements $\langle 23S|r|23P\rangle$ and $\langle 23P|r|24S\rangle$, along with the small energy difference between the $23P$ level and the middle of the $23S$-$24S$ interval (only 6 GHz, see Fig. 3) makes it possible to induce, with available microwave powers, observable two-photon transitions between the $23S$ and $24S$ levels. Furthermore, the precise knowledge of the $23S$-$24S$ transition frequency (obtained by averaging the frequencies corresponding to the $24S$-$23P$ and $23S$-$23P$ transitions) has allowed us to find easily the position of this very narrow resonance, which is exhibited on the recording of Fig. 4(b).

We have observed this two-photon line for microwave powers down to 5.10^{-4} W/cm^2. Its width is of the order of 1 MHz and is probably limited by the BWO frequency instabilities [note the change in scale between Fig. 4(a) and 4(c) and Fig. 4(b)]. The $23S$-$24S$ line is of course less sensitive to Stark effect than the single-photon S-P lines, because it links two S states much less polarizable than the $23P$ level (see Sec. III C).

Notice that the microwave investigation that we present here is quite reminiscent of the well-known high-resolution laser studies on the "$3S$-$3P$-$5S$ triangle" in Na. The $3S$-$3P$, $3P$-$5S$, and two-photon $3S$-$5S$ transitions have been observed in several Doppler-free laser investigations.[9,10] In particular, observation of the $3S$-$5S$ two-photon transition[10] with moderate laser power relies on the same kind of energy coincidence that the one which we have taken advantage of in our microwave studies. Let us recall that the $3S$-$5S$ line is split in two hyperfine components about 800 MHz apart. The corresponding splitting on the $23S$-$24S$ resonance is only of the order of 47 kHz and cannot be observed with our present resolution.

III. SPECTROSCOPIC RESULTS

We give in this section the spectroscopic data we have obtained with our measurements concerning quantum defects, fine structures, and polarizabilities.

A. Quantum defects

All the transitions that we have observed are displayed on the energy diagram of Fig. 5. Their frequencies are summarized in Table I. We do not take into account in this table the fine-structure splittings. These splittings are too small to be observed in the D and F states. For the S-P and D-P transitions, we give in the table the position of the resonance as it would be observed if the fine-structure coupling in the nP states were switched off (see Sec. II E). All the observed resonances correspond to $\Delta l = \pm 1$ electric-dipole-allowed transitions, except the $23S$-$24S$ and the $28D$-$29D$ transitions. The former one is a two-photon $\Delta l = 0$ allowed transition (see Sec. II E). The latter is a single-photon $\Delta l = 0$ transition, which should be in principle forbidden, but which is in fact allowed by the Stark mixing due to the stray electric-field inhomogeneities.[4]

The wavelengths of the $23S$-$24S$ and $28D$-$29D$ transitions have been measured directly. The uncertainties of the corresponding frequencies are ±30 MHz. All other frequencies have been extrapolated between calibrated positions. We assume

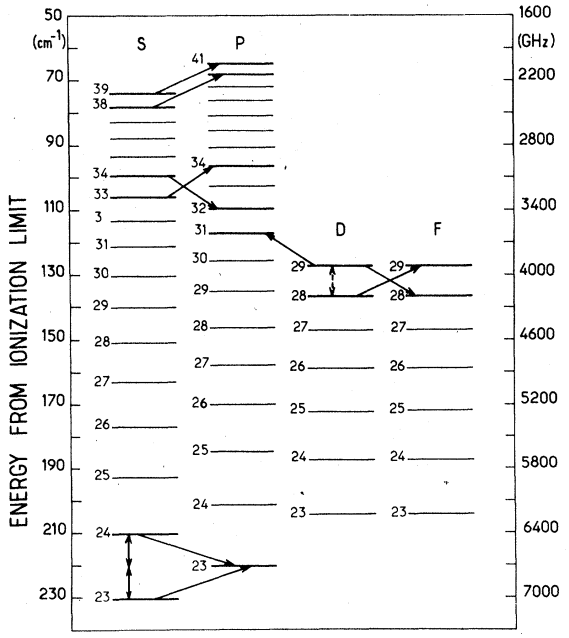

FIG. 5. Part of Na-atom energy diagram displaying all the microwave transitions studied in this paper.

TABLE I. Microwave resonance frequencies observed in this work. First column: measured values (experimental uncertainty ±0.06 GHz except as indicated); second column: frequencies of the same resonances computed from the quantum defects given in Table II.

Line	Measured frequency (GHz)	Computed frequency (GHz)
23S-24S	2 × (302.906 ± 0.03)	2 × (302.907)
23S-23P	308.909	308.862
24S-23P	296.927	296.953
29D-31P	295.577	295.619
28D-29F	288.252	288.286
29D-28F	280.931	280.991
28D-29D	284.825 ± 0.03	284.830
33S-34P	289.102	289.117
34S-32P	305.880	305.824
38S-40P	301.910	301.954
39S-41P	279.265	279.230

their uncertainty is ±60 MHz.

By fitting the measured frequencies to the general Rydberg formula,

$$\nu(nl \rightarrow n'l') = R\left(\frac{1}{(n-\epsilon_l)^2} - \frac{1}{(n'-\epsilon_{l'})^2}\right), \tag{3}$$

one can obtain the values of the quantum defects ϵ_l for the S, P, and D levels. We adopt here the value

$$R = 3\,289\,764 \text{ GHz} \tag{4}$$

for the Rydberg constant taking into account the finite mass of the Na nucleus, and we assume that, within the accuracy of our measurements, the variation with n of the quantum defects cannot be significant.

One can first get values for ϵ_S and ϵ_D by directly inserting into (3) the values obtained for the 23S-24S and 28D-29D intervals. One thus obtains

$$\epsilon_S = 1.3470(10), \tag{5}$$

$$\epsilon_D = 0.0143(7). \tag{6}$$

To get another determination of ϵ_D, one can also rely on the value $\epsilon_F = 0.0016$, which has been previously determined experimentally[1] and theoretically[11] with a very good accuracy.

Using the 28D-29F and 29D-28F measured frequencies, one gets for ϵ_D,

$$\epsilon_D = 0.0144(3) \tag{7}$$

which is consistent with the previous value given by (6). Knowing ϵ_S and ϵ_D, ϵ_P can be determined either from the S–P frequencies, or from the D-P frequency. From the 23S-23P and 24S-23P measurements, one gets

$$\epsilon_P = 0.8541(10) \tag{8}$$

TABLE II. Quantum defects of S, P, and D levels derived from our experimental data.

	Quantum defect
$L=0$	$\epsilon_S = 1.3470^{-0.0007}_{+0.0014}$
$L=1$	$\epsilon_P = 0.8541^{-0.0006}_{+0.0013}$
$L=2$	$\epsilon_D = 0.0144^{-0.0003}_{+0.0004}$

and from the 29D-31P measurement

$$\epsilon_P = 0.8547(7) \tag{9}$$

which are again consistent values. To summarize, we retain the quantum-defect values, which are quoted in Table II. Using these values, we have calculated the "theoretical" frequencies of the various transitions listed in Table I. We see that the differences between computed and observed values lie very well within experimental uncertainties. Our quantum-defect values determined by microwave resonance are in good agreement with those determined by optical transitions. Reference 12 yields, indeed, the values

$$\epsilon_S = 1.348, \quad \epsilon_P = 0.855, \quad \epsilon_D = 0.0148 \tag{10}$$

for n around 10.

B. Fine structures

Fine-structure intervals in six np levels ($n = 23, 31, 32, 34, 40, 41$) have been obtained by measuring the splittings of the S-P and P-D resonance lines. The measured intervals are given in Table III. The accuracy of the measurements is limited by the precision in the knowledge of the frequency-versus-voltage BWO calibration. All the fine-structure intervals are positive (i.e., the $P_{3/2}$ component lies above the $P_{1/2}$ one). This is easy to check by identifying the $P_{3/2}$ line Stark splitting (see Sec. III C). We have plotted on a logarithmic scale, on Fig. 6, the measured fine-structure intervals as a function of n^*, where $n^* = n - \epsilon_P$ is the effective quantum number. We have reported on

TABLE III. Fine-structure intervals measured in this work.

n	Fine-structure interval (MHz)
23P	493 ± 18
31P	221 ± 30
32P	157 ± 30
34P	129 ± 30
40P	82 ± 30
41P	99 ± 30

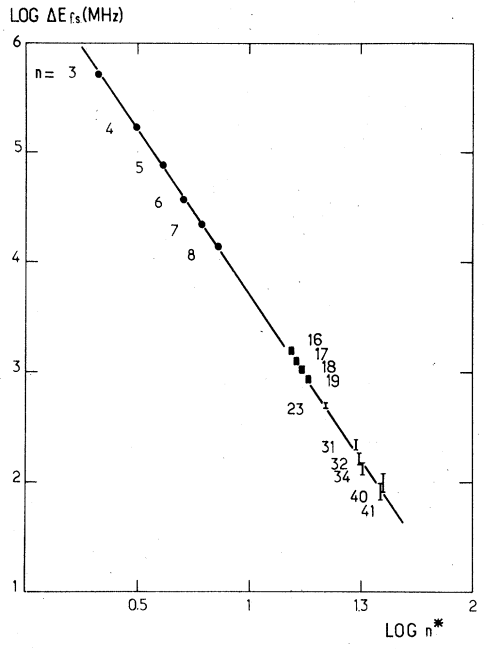

FIG. 6. nP fine-structure interval (in MHz) as a function of the effective quantum number in log-log diagram, for low-lying levels (Ref. 13), intermediate levels (Ref. 7), and very excited states (this work).

the same plot the fine-structure intervals measured in lower nP states ($n = 3$–8) on optical transitions,[13] and the intervals recently measured by radio-frequency spectroscopy on intermediate excited states[7] ($n = 16$–19). We see that all the fine-structure intervals obey rather well the same n^{*-3} law.

C. Polarizabilities

We have observed the Stark effect of all the above-mentioned transitions by applying on the atoms a small calibrated dc electric field.

The Stark diagram of a Rydberg level depends upon the order of magnitude of the applied field: for electric field $\mathcal{E}$ below a critical value $\mathcal{E}_c$, the Stark shift is quadratic. For $\mathcal{E} \gg \mathcal{E}_c$, it becomes linear like in hydrogen. The critical field $\mathcal{E}_c$ is such that the Stark shift is of the order of the gap between nearby levels of opposite parity. $\mathcal{E}_c$ varies like $n^{-5} \times l^{-6}$, and decreases rapidly within a given n shell, when l is increased.[11]

We have shown in a previous letter[4] that the stray field acting on the atoms in our experiment (~0.1 V/cm) is larger than $\mathcal{E}_c$ for states $n \sim 30$ and $l > 2$ and thus makes it very difficult—if not impossible—to observe the quadratic regime for those states; we have already discussed some results concerning the linear Stark regime for such levels.[4] In this paper, we are interested in the quadratic regime, which can be described in terms of atomic polarizabilities. We have thus restricted our study to S and P states.

For S levels, the Stark shift ΔE is

$$\Delta E = -\tfrac{1}{2}\alpha_{0S}\mathcal{E}^2 . \tag{11}$$

It is determined by a single parameter, namely the scalar polarizability α_{0S} of the level.

For P levels, and if the electric field $\mathcal{E}$ is weak enough so that it does not decouple the spin-orbit interaction, the shift ΔE_{nPJM_J} of a given $|nPJM_J\rangle$ fine-structure state can be obtained from the general formula[14]

$$\Delta E_{nlJM_J} = -\tfrac{1}{2}\alpha_{0nl}\mathcal{E}^2 - \tfrac{1}{2}\alpha_{2nlJ}\frac{3M_J^2 - J(J+1)}{J(2J-1)}\mathcal{E}^2 , \tag{12}$$

where α_{0nl} and α_{2nJ} are, respectively, the scalar and tensor polarizabilities. Since we measure only energy differences between Rydberg states, we are able to determine in that way the differences between the polarizabilities of the two states linked by the microwave transition. If these polarizabilities differ by more than one order of magnitude, we can nevertheless get a good determination of the larger one.

TABLE IV. S- and P-level polarizabilities in Na. The values are the ones measured in this work, except when indicated otherwise. Both scalar and tensor polarizabilities are given for P levels. Figures in brackets correspond to theoretical values. All polarizabilities are expressed in MHz/(kV/cm)^2.

	α_{0S}	α_{0P}	α_{2P}
$n=3$	0.0396 [a]	0.089 [b]	−0.017 [b]
$n=5$	5.2 [a]		
$n=6$	23.6 [a]		
$n=7$	76.4 [a]		
$n=8$	206 [a]		
$n=17$			3.2×10^4 [c]
$n=18$			5.0×10^4 [c]
$n=19$			7.4×10^4 [c]
$n=23$	$\alpha_{24S}-\alpha_{23S}$	-4.2×10^6	4.6×10^5
	$=9.9\times10^4$	$[-3.5\times10^6]$	$[3.4\times10^5]$
$n=24$	$[9.1\times10^4]$		
$n=32$		-38.6×10^6	3.7×10^6
		$[-41\times10^6]$	$[4.0\times10^6]$
$n=34$		-75.4×10^6	8.2×10^6
		$[-64\times10^6]$	$[6.4\times10^6]$
$n=41$		-325×10^6	
		$[-262\times10^6]$	

[a] Reference 15 and references therein.
[b] Reference 14.
[c] Reference 7.

1. S level polarizabilities

We have measured the quadratic shift of the two-photon $23S$-$24S$ resonance in increasing electric fields ranging from 0 to 35 V/cm. We have thus obtained the difference between the scalar polarizabilities of the $23S$ and $24S$ levels given in Table IV.

2. P level polarizabilities

By studying the shifts and splittings of S-$P_{1/2,3/2}$ transitions, we have obtained the scalar and tensor polarizabilities of the P levels. These P levels have indeed a much larger Stark effect than the corresponding S ones, so that one can completely neglect the contribution of the S level in the shift of the S-P line. We give in Table IV the measured scalar and tensor polarizabilities of nP levels ($n = 23, 32, 34, 41$). Note that we do not have the polarizability of the $31P$ level. As we have in fact observed it through a D-P transition (see Fig. 5), the Stark shift of the corresponding line reflects essentially the D-level perturbation and does not yield a precise value for the P-level polarizability.

There is a tremendous difference (up to ten orders of magnitude) between the polarizability of Rydberg levels and those of the low excited states. This can be seen in Table IV, in which we have included several results concerning lower S and P states,[7,14,15] some of which have been recently obtained by optical double-photon transitions,[15] and by radio-frequency spectroscopy.[7] The accuracy of our polarizability measurements is of the order of ±10%.

We compare in the same table our experimental data to theoretical values calculated from a Coulomb approximation[16] (figures in brackets are below the experimental values). The agreement between experiment and theory appears to be good. This confirms[14,15] that the Rydberg levels behave in a hydrogenic way in so far as their polarizabilities are concerned.

IV. CONCLUSION

The experiments reported in this article illustrate the possibilities of the selective-field-ionization technique in double-resonance millimeter studies of atomic Rydberg levels.

It is clear that, even with the present moderate resolution, a lot of other spectroscopic investigations of interest can be developed, in other alkali or alkaline-earth Rydberg levels. In this latter case, quantum defect measurements by millimeter spectroscopy would yield, for example, valuable information on the polarization of the open shell of the core by the valence electron.

However, an increase in the precision of the experiments is desirable for spectroscopic and metrologic applications as well. In order to achieve this goal, several improvements of the experimental setup are presently under progress, including (i) a stabilization of the microwave generator and a direct measurement of its frequency, (ii) a better shielding of the stray electric field in order to allow access to high angular-momentum levels, (iii) a lengthening of the atom-microwave interaction time in order to reduce the intrinsic width of the resonances.

The first improvement is certainly easy to achieve, but the extent to which it will contribute to increase the resolution obviously depends on the ultimate improvements which could be made at the same time in points (ii) and (iii). This is still an open question. In particular, the distance along which an excited atom in a well-defined Rydberg level could be propagated in a beam without perturbation depends on the ultimate electric-field shielding which could be realized and on lifetime and collisional properties of these atoms which are not yet well known. Improvements in spectroscopic resolution involve not only technological advances, but also further developments of experimental and theoretical studies on Rydberg states. We hope that the experiments reported here will stimulate new efforts in these fields and open the way to a new domain of ultrahigh-resolution studies.

[1]T. F. Gallagher, R. M. Hill, and S. A. Edelstein, Phys. Rev. A 13, 1448 (1976).
[2]K. B. MacAdam and W. H. Wing, Phys. Rev. A 15, 678 (1977), and references therein.
[3]D. Kleppner, Bull. Am. Phys. Soc. 20, 1458 (1976).
[4]C. Fabre, P. Goy, and S. Haroche, J. Phys. B 10, L183 (1977).
[5]T. W. Ducas, M. G. Littman, R. R. Freeman, and D. Kleppner, Phys. Rev. Lett. 35, 366 (1975).
[6]R. V. Ambartsumyan, G. I. Bekov, V. S. Letokhov, and V. I. Mishin, Zh. Eksp. Teor. Fiz. Pis'ma Red. 21, 595 (1975) [JETP Lett. 21, 279 (1975)].
[7]T. F. Gallagher, L. M. Humphrey, R. M. Hill, W. E. Cooke, and S. A. Edelstein, Phys. Rev. A 15, 1937 (1977).
[8]D. H. Tuan, S. Liberman, and J. Pinard, Opt. Commun. 18, 533 (1976).
[9]P. Jacquinot, in *High-Resolution Laser Spectroscopy*, edited by K. Shimoda (Springer-Verlag, Berlin, 1976), p. 52 and references therein.

[10]F. Biraben, B. Cagnac, and G. Grynberg, Phys. Rev. Lett. 32, 643 (1974); M. D. Levenson and N. Bloembergen, Phys. Rev. Lett. 32, 645 (1974).
[11]R. R. Freeman and D. Kleppner, Phys. Rev. A 14, 1614 (1976).
[12]I. Johansson, Ark. Fys. 15, 169 (1958); P. P. Risberg, Ark. Fys. 10, 583 (1956).
[13]C. Moore, *Atomic Energy Levels*, NSRDS-NBS No. 35 (U.S. GPO, Washington, D.C., 1971), Vol. I.
[14]R. W. Schmieder, A. Lurio, and W. Happer, Phys. Rev. A 3, 1209 (1971).
[15]R. T. Hawkins, W. T. Hill, F. V. Kovalski, A. L. Schawlow, and S. Svanberg, Phys. Rev. A 15, 967 (1977).
[16]The Coulomb approximation calculation has been widely used since Bates and Damgaard's classic paper [Philos. Trans. R. Soc. London 242, 101 (1949)]. It consists in calculating dipolar radial matrix elements between nl and $n'l'$ states as a series expansion truncated to the $(n+n')^2/2$ first terms. Because of the large number of very large terms of opposite signs in this series, computer round-off errors limit this simple method to about $n=20$ (when using double precision). To obtain the polarizabilities of the Rydberg levels of interest, we have systematically computed the polarizabilities of $n=3$ to $n=20$ levels and extended the results to higher n values by a logarithmic extrapolation. S-level polarizabilities vary nearly like n^{*6}, whereas P-level polarizabilities obey a more complicated power law, with several parameters in the exponent.